Geological characterisation guided by fuzzy k-means clustering of physical properties measured from core samples from the Victoria property, Sudbury Ontario

by

Jacqueline Huggins

A thesis submitted in partial fulfillment
of the requirements for the degree of
Master of Science (MSc) in Geology

The Faculty of Graduate Studies
Laurentian University
Sudbury, Ontario Canada

THESIS DEFENCE COMMITTEE/COMITÉ DE SOUTENANCE DE THÈSE
Laurentian Université/Université Laurentienne
Faculty of Graduate Studies/Faculté des études supérieures

Title of Thesis
Titre de la thèse: Geological characterisation guided by fuzzy k-means clustering of physical properties measured from core samples from the Victoria property, Sudbury Ontario

Name of Candidate
Nom du candidat: Huggins, Jacqueline

Degree
Diplôme: Master of Science

Department/Program
Département/Programme: Geology

Date of Defence
Date de la soutenance August 14, 2018

APPROVED/APPROUVÉ

Thesis Examiners/Examinateurs de thèse:

Dr. Richard Smith
(Co-Supervisor/Co-directeur de thèse)

Dr. Doug Tinkham
(Co-supervisor/Co-directeur de thèse)

Dr. Stephen Gregory
(Committee member/Membre du comité)

Dr. Rob Shivers
(Committee member/Membre du comité)

Dr. Christian Dupuis
(External Examiner/Examinateur externe)

Approved for the Faculty of Graduate Studies
Approuvé pour la Faculté des études supérieures
Dr. David Lesbarrères
Monsieur David Lesbarrères
Dean, Faculty of Graduate Studies
Doyen, Faculté des études supérieures

ACCESSIBILITY CLAUSE AND PERMISSION TO USE

Abstract

Core logging is a subjective practice done by geologists, which documents the mineralogy, textures, alteration, mineralisation and other features to give core a rock name. Pattern recognition techniques are able to characterise the rocks and link the geophysical and geological data quantitatively. The fuzzy-k means algorithm is an unsupervised pattern recognition technique, which groups data into clusters based on properties measured. This study will use the fuzzy-k means algorithm to characterise core samples from 2 drillholes from the Victoria property in Sudbury with thin section examination to identify how mineralogical changes can affect the measurements. Four different physical properties (density, gamma ray, conductivity and magnetic susceptibility) were measured from a total of 203 core samples of quartz diorite, metagabbro, metabasalt, pyroxenite, olivine diabase and metasedimentary rocks. The samples were classified into 4 different physical units, with additional confusion index values that indicate how well the data was classified. Quartz diorite, metagabbro and metabasalt have the highest confusion index values while the olivine diabase and metasedimentary rocks have the lowest confusion index values. Combining the fuzzy k- means results and thin section examination proved to be successful because heterogeneities in sulphide minerals, ore mineralisation and variation in rock forming minerals cause an overlap in physical properties with other rock samples, increasing the confusion index while homogeneity in mineralogy results in a low confusion index.

Keywords

Fuzzy k-means algorithm

Confusion index

Physical property

Acknowledgements

I will have to start off first by thanking my supervisors Drs. Richard Smith and Doug Tinkham for their help with my project from Dr. Smith helping with all the geophysical knowledge and the idea for the project and Dr. Tinkham for helping in the field all summer and applying his wealth of knowledge in the geological portion of the project. I'd like to thank Robert Shives from GamX Inc. for his wealth of knowledge on gamma ray spectrometry during the project and Ronald Martin from Radiation Solutions for supplying the Gamma Ray spectrometer and helping with understanding how to use the equipment. Steven Gregory and Bill Spicer with all the help from KGHM.

Secondly, I'd like to thanks NSERC Research Chair for funding my project, as well as KEGS and CSEG for additional funding.

Thirdly, thanks to numerous individuals at the Harquail School of Earth Science: Sydney Albert for being a fantastic field partner in helping collect all the data for my project and my classmates and officemates: Christopher Kelly, Francisca Maepa, Nikolas Gazo, Frédéric Gaucher and Yongxing Li. In particular, Philippe Trudel, you've been over and beyond supportive and I can't thank you enough!

Last and certainly not least, I want to thank my family for their support during my 6 years at Laurentian, in particular my mom, who was my biggest supporter. I'm dedicating this to her.

Table of Contents

List of Tables

List of Figures

1 Introduction

Drill core logging is the practice of observing and recording information about a rock, which includes determining the lithology, noting features of interest and may include measurement and recording of physical properties. This is achieved by visually identifying the mineralogy and textures of the sample and giving the rock a name using a classification system. Classifying rocks using visual estimates of the percentage of minerals and textures is a subjective practice, such the resulting rock names assigned by different observers may vary. Geophysical data can support geological core logging by measuring the physical properties of the rock and thus aid in predicting the rock type. However, as physical properties of most rocks span a range of values, there can be an overlap of physical properties, which introduces confusion to the lithology prediction (Mahmoodi et al., 2015). Some of this rock property variation can be related to mineralogical variations within a given rock type.

Borehole logging methods provide rock property data and visual information. Pattern recognition techniques have been applied to borehole data where there is little to no core recovery to deduce the nature of the surrounding rocks (Benaouda et al., 1999). Conversely, these techniques have been applied to boreholes where there is core recovery to characterise the rocks and link the geophysical and geological data quantitatively.

Fuzzy k-means clustering is an unsupervised classification technique that searches for patterns in data by grouping the data into clusters so that the data in each cluster is similar to each other, yet differs from the other clusters (Žalik, 2008). Since there can be an overlap of physical properties amongst different lithologies, rock samples can belong to more than one cluster, reducing the

accuracy of predicting the rock type from the cluster information. Previous studies using the fuzzy k-means clustering algorithm have been applied to physical data collected in downhole geophysical logs from boreholes in the Sudbury area to characterise rock types (Mahmoodi, 2016). However, since geological differences (mineralogy, textures, alteration) amongst different lithologies are important in placing data into clusters, collecting samples and observing the geological changes helps in understanding why there is heterogeneity and thus low accuracy in predicting rock types.

Clustering of downhole physical property data from the Victoria property in Sudbury using the fuzzy k-means clustering algorithm method from Mahoomdi (2016) was successful, with potential usage in mineral exploration. Similarly, this study will characterise samples from 2 drillholes from the Victoria property using gamma-ray, magnetic susceptibility, density and conductivity data with the fuzzy k-means clustering algorithm. This study differs from that of Mahmoodi (2016) by using core samples rather than downhole logs and additionally integrating petrological observations with all the physical measurements to identify how mineralogical changes can affect the measurements. Furthermore, instead of using total gamma-ray count (as was done for the downhole logs), this study utilises concentration estimates of K, eU and eTh derived from data collected using a portable gamma-ray spectrometer (GRS) to determine if element-specific assays yield more information than total counts.

2 Geological setting

2.1 Study area

The Sudbury Igneous Complex (SIC) is a 1.85 Ga meteorite impact crater geographically divided into the north, east and south range (Rousell and Card, 2009). This study focuses on the southwestern corner of the SIC on the Victoria property, owned by KGHM International Limited (KGHM). The Victoria property is located along the southwestern side of the Sudbury basin, about 35 km from Sudbury (Spicer, 2016). The property has produced nickel, copper and platinum group minerals (PGM) from pyrrhotite, pentlandite and chalcopyrite sulphide ore hosted within quartz diorite (Spicer, 2016). Drillholes FNX 1182 and FNX 1168 were selected for this study because they intersected a variety of lithologies (figure 1) and all core was readily available.

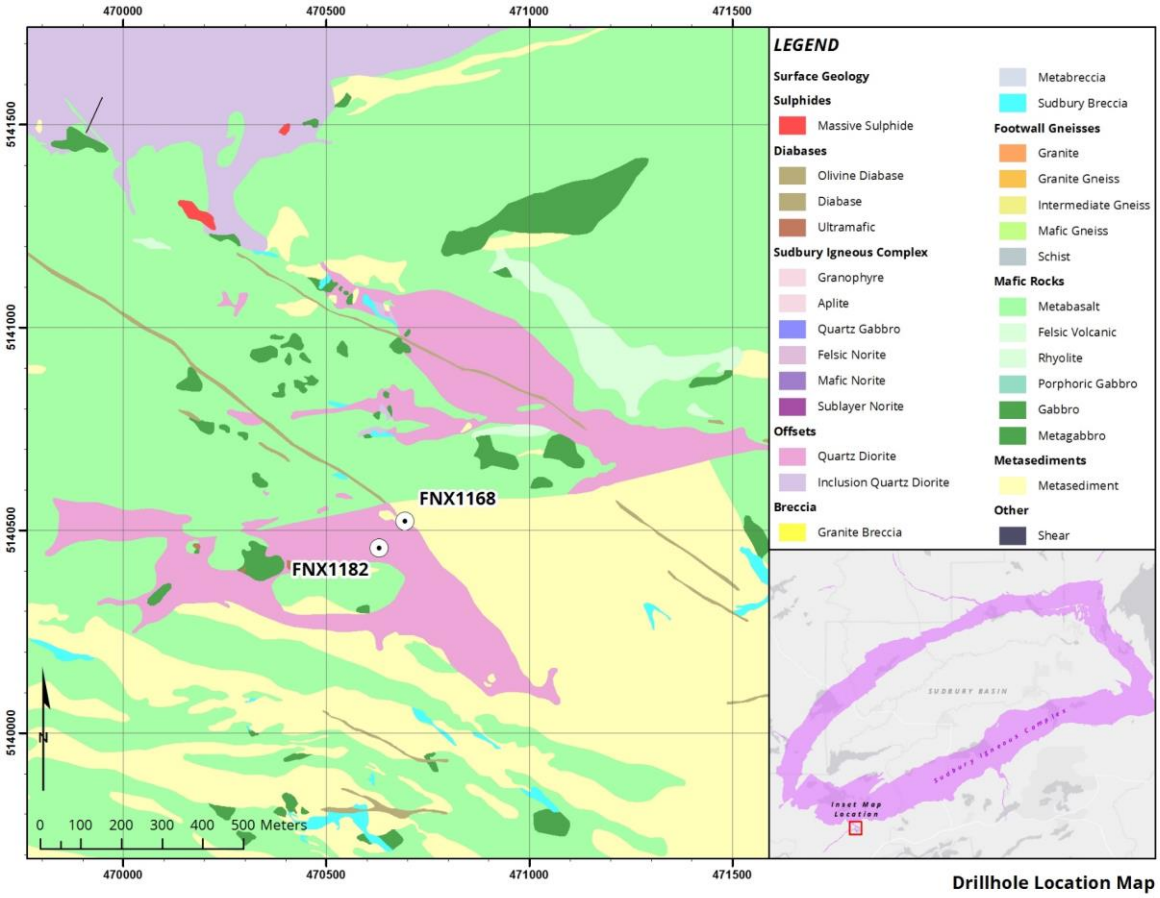

Figure 1: Victoria property map with drillholes FNX 1168 and FNX 1182 (Courtesy of Steven Gregory and Nicholas Moylan)

3 Methodology

3.1 Measurement procedures

Four different parameters were measured on each piece of core: density, magnetic susceptibility, conductivity, and gamma-ray spectrometry assays of K, eU and eTh. A minimum of three core samples were measured from each core box, about 1 to 1.5 m downhole from each other, dependent on core availability. Where lithology appeared more variable, four to five core samples were taken from individual core boxes for measurement.

3.1.1 Density

To determine the density of the core sample, the whole core piece measured in the field was brought to the Willet Green Miller Centre to measure the bulk density using Archimedes' principle. Each core sample was weighted on a tray on top of an Ohaus Adventurer Pro scale in air and then suspended from a hook at the bottom of the scale and weighed while submerged in water (figure 2). Both weights were recorded and bulk density was measured using equation (1).

$$\text{Density } (g/cm^3) = \text{weight in air} / (\text{weight in air-weight in water}) \quad (1)$$

3.1.2 Magnetic susceptibility and conductivity

Magnetic susceptibility was measured in the field with a Terraplus KT-10 S/C magnetic susceptibility meter (Terraplus Inc.) and conductivity was measured with a GDD instruments MPP EMS2 probe (Instrumentation GDD Inc.). For both parameters, each core sample was measured in 5 spots and an average was calculated for each core sample.

Figure 2: Density measurement while core is submerged in water

3.1.3 Gamma ray spectrometer (GRS)

An RS-330S portable gamma ray spectrometer supplied by Radiation Solutions Inc. was used to measure the gamma-ray spectrum of rock obtained from drill core samples. The readings in specific energy windows are then converted to GRS assays using standard procedures (IAEA, 2003). Figure 3 shows the spectrometer set up in the field with lead shielding around the detector and the core to reduce background counts. Three spots on the core (each end and the middle) were measured three times. Before measurements are taken, the spectrometer is powered on and it then takes about 10 minutes for self-calibration, where the unit automatically sorts gamma ray energies associated with naturally occurring isotopes K-40 (1.46 MeV), Bi-214 (1.76 MeV) and Tl-208 (2.62 MeV) into pre-defined spectral channels. This calibration data is used to adjust the energy calibration (using natural sources) and to establish a background in the area.

All subsequent measurements have this background subtracted. Then a yellow rod is inserted into the position in the lead shield where the core will be put. The yellow rod is made of aluminum, which contains trace potassium, uranium and thorium, assumed to be too low to measure. The rod is used rather than air, as the rod has a density comparable to rock and will adsorb a similar number of gamma rays coming from the ground as the core samples do. Hence, when the rod is measured, the readings should be zero or statistically close to zero. Extra caution was taken in ensuring there were very little background gamma rays from the sky and ground by adjusting the positions of the lead shielding around the spectrometer.

Figure 3: Radiation Solutions RS-330S gamma ray spectrometer in the field, placed into five rings of lead surrounding the spectrometer sensor, sitting on additional lead bricks used to create a core-measurement chamber. The lead is dense, and is used to reduce gamma-rays from all non-drill core sources, including cosmic atmospheric and nearby ground sources.

3.1.4 Petrology

When the physical properties readings were significantly different or anomalous (>20% variance) from surrounding readings, or the rock has variability in geological features (mineralisation, alteration, inclusions), samples were collected for subsequent thin section examination in order to better understand the geological and mineralogical changes. In addition, representative samples of each rock type identified were collected for thin section examination to compare to anomalous samples.

3.2 Effect of core length on gamma-ray spectrometer readings

All gamma ray spectrometers that provide concentration estimates are calibrated for that purpose assuming the readings will be taken on a similar type of material (rocks, for example) and with similar geometry (flat outcrop surface for example). Application to drill core measurement as described in this study does not match the source calibration geometrically, as the drill core represents a much smaller source volume relative to a flat outcrop, which typically is considered to represent a 0.3 cubic meters.

In addition, because some of the detected gamma rays emanate from the end of the drill cores lying outside the measurement chamber, selection of a core sample with an appropriate core length is important for this study. A series of tests were undertaken on different lengths of core to determine how gamma-ray measurements from the middle of the core are affected by the core length. Six long samples of core (35-39 cm) were selected from 6 different core boxes and measured with the gamma ray spectrometer for 3 minutes. To determine the dependency of gamma-ray counts on length of core, about 5 cm of core was removed from both sides of the

same piece of core to create shorter core (~24-27 cm) and the sample was remeasured. The mean and standard deviation were calculated and Table 1 shows the results. Measurements shown in green are omitted from the analysis because the measurements are zero for one length and cannot be compared. If the long and short core have readings that are statistically similar (the readings plus or minus the standard deviation overlap), we can conclude that the characterisation of the core samples is the same; however, three out of the four core samples have lower readings in the longer core (shown in red). This is unexpected, as the longer core has more material and should have more gamma-rays emitted. As they do not, we know that the lower readings from long core are a consequence of statistical variability and not a consequence of the change in the volume of rock. They can be ignored, as they are not helping to determine the effect of changes in volume. The six remaining samples (shown in blue) show that the short samples have statistically similar readings to the longer samples. Given the variable nature of the readings, it is concluded that the short samples are valid to take measurements for the project. The length of core used for this project ranges from 21 to 26 cm.

3.3 Background readings after rain

Rainfall fills pore space in soil and pushes out radon that might have settled in the pore space, and this radon is radioactive and can adversely impact the readings. Hence it is not recommended to use the spectrometer within 12 hours of rainfall. A series of test were done after rainfall with an aluminum rod to see the effects of rain on the shielded spectrometer used in this thesis. Table 2 shows the results of these tests. In all cases, the assays are small or close to zero, therefore it was concluded that measurements could continue after rain. This is a testament to the ability of the lead to shield gamma-rays associated with background and radon.

Furthermore, in order to get reliable readings, the spectrometer was not used in the early mornings to avoid the effects of radon gas emitted from the soil overnight, giving unreliable eU readings. Therefore, the spectrometer was only used after 11am.

Row 1 Box 12									
Length=35.5 cm		St.dev	Mean + St. dev.	Mean – St. dev.	Length=24.4 cm		St. dev.	Mean + St. dev.	Mean - St.dev
K (%)	0.46	0.09	0.55	0.37	K (%)	0.49	0.09	0.58	0.4
eU (ppm)	0	0	0	0	eU (ppm)	1.1	0.4	1.5	0.7
eTh (pm)	3.6	1.0	4.6	2.6	eTh (ppm)	2.8	1.0	3.8	1.8
Row 2 Box 12									
Length=35 cm		St. dev.	Mean + St. dev.	Mean - St.dev	Length=27.4 cm		St. dev.	Mean + St. dev.	Mean - St.dev
K (%)	0	0	0	0	K (%)	0.44	0.09	0.53	0.35
eU (ppm)	0	0	0	0	eU (ppm)	1.5	0.4	1.9	1.1
eTh (ppm)	1.9	1.1	3.0	0.8	eTh (ppm)	0	0	0	0
Row 1 Box 5									
Length=32.5 cm		St. dev.	Mean + St. dev.	Mean - St.dev	Length=25.3 cm		St. dev.	Mean + St. dev.	Mean - St.dev
K (%)	0.21	0.09	0.3	0.12	K (%)	0	0	0	0
eU (ppm)	0	0	0	0	eU (ppm)	0	0	0	0
eTh (ppm)	6.3	1.1	7.4	5.2	eTh (ppm)	4.2	1.1	5.3	3.1
Row 3 Box 13									
Length=35.5 cm		St. dev.	Mean + St. dev.	Mean - St.dev	Length=24.4 cm		St. dev.	Mean + St. dev.	Mean - St.dev
K (%)	0.46	0.09	0.55	0.37	K (%)	0.41	0.1	0.51	0.31
eU (ppm)	0	0	0	0	eU (ppm)	1.2	0.5	1.7	0.7
eTh (ppm)	3.7	1.0	4.7	2.7	eTh (ppm)	3.2	1.1	4.3	2.1
Row 2 Box 13									
Length=37.5 cm		St. dev.	Mean + St. dev.	Mean - St.dev	Length=24.4 cm		St. dev.	Mean + St. dev.	Mean - St.dev
K (%)	0.2	0.1	0.3	0.1	K (%)	0.55	0.1	0.65	0.45
eU (ppm)	0	0	0	0	eU (ppm)	0	0	0	0
eTh (ppm)	3.6	1.0	4.6	2.6	eTh (ppm)	2.9	1.0	3.9	1.9
Row 3 Box 7									
Length=39 cm		St. dev.	Mean + St. dev.	Mean - St.dev	Length=24.4 cm		St. dev.	Mean + St. dev.	Mean - St.dev
K (%)	0.21	0.09	0.3	0.12	K (%)	0.45	0.09	0.54	0.36
eU (ppm)	0	0	0	0	eU (ppm)	0.6	0.4	1	0.2
eTh (ppm)	1.5	1.0	2.5	0.5	eTh (ppm)	2.7	1.0	3.7	1.7

Table 1: Gamma-ray spectrometry assays from 6 core boxes comparing the "long core" and the "short core".

Test #	1	2	3	4	5
K (%)	0.28+/- 0.07	0.12+/- 0.07	<0	<0	<0
eU (ppm)	<0	<0	<0	0.9+/-0.3	<0
eTh (ppm)	<0	0.9+/-0.8	1.5+/-0.8	<0	<0

Table 2: Gamma-ray spectrometer test after rainfall with an aluminum rod

3.4 Empty chamber tests

Five tests were done with the core chamber empty without core or an aluminum rod to test the readings of the gamma ray spectrometer. Once again the readings are small and effectively zero (Table 3).

Test #	1	2	3	4	5
K (%)	0	0	0	0	0.5+/-0.09
eU (ppm)	1.1+/-0.4	0.9+/-0.4	0.4+/-0.3	0	1.1+/-0.4
eTh (ppm)	2.0+/-1.0	0	0	0	0

Table 3: Gamma-ray spectrometer test with an empty core chamber

3.5 Fuzzy-k means clustering analysis calculation

The fuzzy-k means clustering analysis is an unsupervised classification technique that separates the data into different clusters where the members of a particular cluster have similar measured physical properties (Mahmoodi and Smith, 2015). Each data point, or each sample measured, is able to belong to more than one cluster based on the membership value, which defines how much the data belongs to a cluster. If the membership value for one cluster is zero, or small, then this indicates the sample does not belong to the cluster, but when the membership value of a cluster is closer to one, this indicates that the sample has a stronger membership in the cluster (Mahmoodi and Smith, 2015). Along with membership values, the output from the algorithm includes the confusion index. The confusion index defines how well the sample is classified, ranging between

0 and 1, where 0 is a perfectly defined sample with a membership value in one cluster close to one. A larger confusion index indicates that the sample has membership values that are significant for two or more clusters. Figure 4 is a histogram of the confusion index values that helps to understand the significance of the confusion index value. The distribution shows a bimodal distribution, with one mode having values between 0 and 0.4 and the second mode lying between 0.7 and 0.9. For the remainder of the paper, "low confusion" refers to samples with an index between 0 and 0.4 and "high confusion" refers to an index between 0.7 and 1.0.

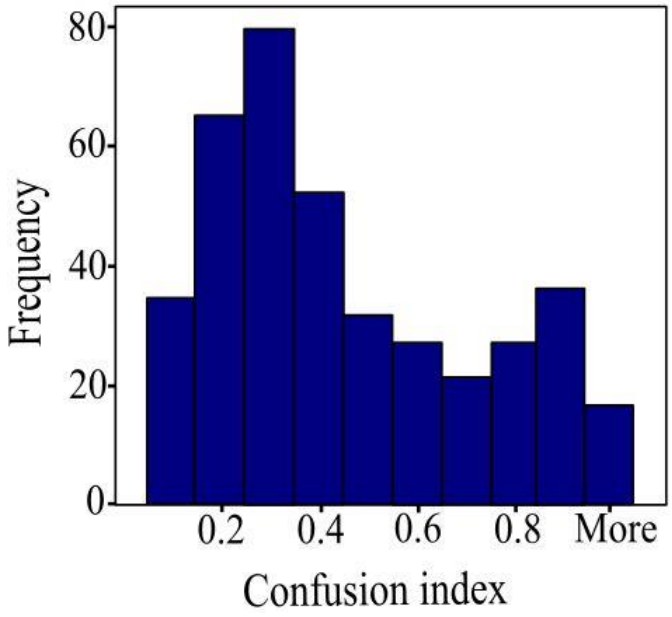

Figure 4: Histogram showing bimodal distribution of low confusion (0.2-0.4) and high confusion (0.7-1.0)

The confusion index was the primary tool used to indicate zones that were geologically interesting as the physical properties are anomalous and indicate some heterogeneities, or unusual character of the lithology. Mahmoodi and Smith (2015) formulated a workflow when using fuzzy k-means for classifying physical properties of data collected from downhole logging. The workflow involves the primary steps of pre-processing the data (removing extraneous values), performing the fuzzy k-means clustering (after determining the optimal number of

clusters), organizing the data into physical units based on maximum memberships and then refining the rock classification in areas with a high confusion index by manually placing the data in one of the following categories:

1) Local heterogeneity: If there are no significant variations in physical properties, and the physical unit is similar above and below.
2) Create a new class: Physical properties are unique, but in small numbers to not warrant the creation of a statistically identifiable class.
3) Transition zone: Physical properties are gradually changing spatially, thus the rock is changing gradually from one physical unit to another. This zone is defined by the gradual increase/decrease in two or more membership values.
4) Intermediate zone: Zone is narrow and shows gradual changes in physical properties, but lies between two less confused units. This zone is reclassified as one of the less confused units above or below it.

4 Results

Each cluster from the k-means clustering is called a "physical unit" as the clusters group together rocks with similar physical properties. Linking the physical units to one or more rock types and placing high confusion data into categories will be discussed in this section. A total of 392 core samples from two drills holes were measured for all 6 physical parameters. There are 203 samples previously classified by a geologist as quartz diorite (including inclusion quartz diorite), 76 as metagabbro, 61 as metabasalt, 18 as metasediment, 12 as pyroxenite, and 12 as olivine diabase. The last 10 samples measured were small units of metabreccia, contorted schist and volcanoclastic rocks.

4.1 Core sample data

The averages for each measured parameter is outlined in Table 4.

Logged rock type	**Density (g/cm^3)**	**K (percent)**	**eU (ppm)**	**eTh (ppm)**	**Total count**	**Log magnetic susceptibility**	**Conductivity (S/m)**
Quartz diorite	2.87	0.38	0.98	2.26	1729.0	-0.083	11.57
Inclusion quartz diorite	2.91	0.40	0.99	2.03	1924.3	-0.045	0
Metagabbro	3.01	0.29	0.99	2.22	1797.7	0.031	0.0026
Metabasalt	3.03	0.19	0.50	1.71	1526.3	0.035	13.70
Metasediment	2.82	1.58	3.23	9.00	2705.9	-0.48	0
Pyroxenite	3.07	0.071	0.84	0.59	1521.5	0.11	0
Olivine diabase	3.06	0.32	0.38	1.09	1289.3	1.81	0

Table 4: Averages for each parameter when classified by rock type

The conductivity measurements were not useful in the fuzzy k-means clustering procedure because they measured 0 S/m for majority of the samples, with exception of the highly mineralised (pyrrhotite, chalcopyrite, pyrite) core samples from quartz diorite, metagabbro and metabasalt.

4.2 Relationship between physical units and rock types

Boxplots are used to summarise the physical properties distribution for each rock type and physical unit or cluster (figure 5). The most homogenous rocks are the olivine diabase (OLDIA) with all parameters, showing very low variance. The metasediment (MTSD) is relatively homogenous in density and shows a slightly larger variation in magnetic susceptibility, but has a wider distribution of values in the three GRS assays (K, eU, eTh). The quartz diorite and inclusion quartz diorite has variations mostly with magnetic susceptibility and more homogeneity with gamma and density. Lastly, metagabbro (MTGB), metabasalt (MTBS) and pyroxenite (PYRT) show relativity homogenous units with small heterogeneities and some outliers in magnetic susceptibility. Table 5 shows the different clusters in each column and how each rock type is distributed among each cluster.

.

Rock types	Cluster 1	Cluster 2	Cluster 3	Cluster 4
Quartz diorite and inclusion QD	-	35	48	120
Olivine Diabase	12	-	-	-
Metagabbro	-	17	48	11
Metabasalt	1	-	51	9
Pyroxenite	-	-	10	2
Metasediment	-	15	1	2
Total	13 (100%)	67 (100%)	158 (100%)	144 (100%)

Table 5: How the different clusters are made up of different rock types (number of samples and percentage) for FNX 1168 and 1182. Red indicates percentages greater than 60%, green between 30 and 60%, blues between 10 and 30% and orange less than 10%.

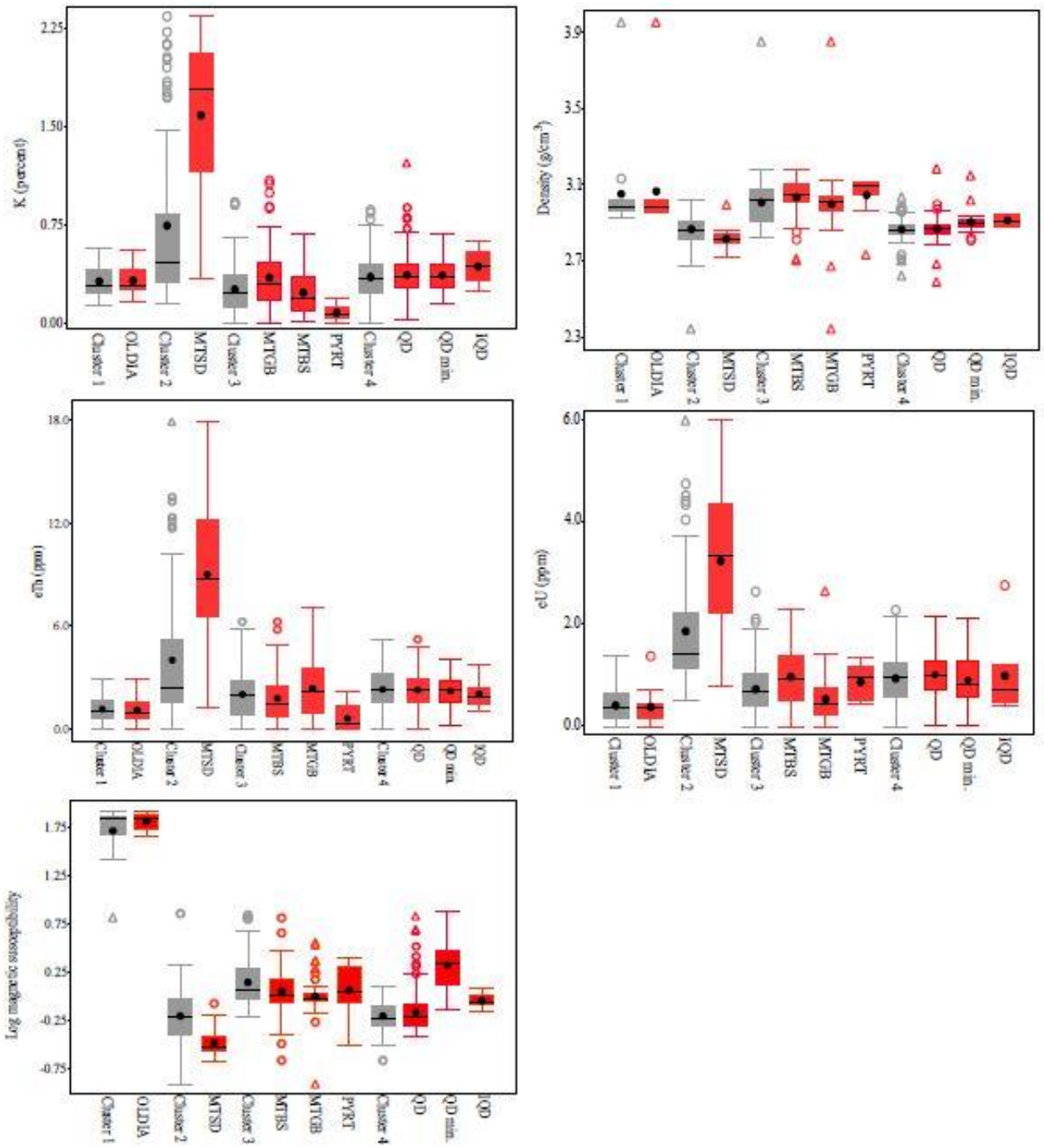

Figure 5: Boxplots of K, eU, eTh, density and magnetic susceptibility for each physical units and rock type for FNX 1168 and 1182.

Olivine diabase seems to be consistently classified into cluster 1, and cluster 4 is primarily quartz diorite (QD) (and inclusion quartz diorite, IQD), although QD and IQD rocks also seem to fall

into clusters 2 and 3, which are the classes most of the other rock types all fall into. The main difference between clusters 2 and 3 is that metasediment falls only into cluster 2 and cluster 2 seems to be characterized by higher K, eU and eTh. If there were more samples of metasediment, cluster 2 might be more clearly defined by the metasediment.

4.3 Physical variations in core samples

The optimum number of clusters for grouping the physical properties measurements taken on the core samples was determined to be four. This number was determined prior to conducting the fuzzy k-means calculations and is objectively based on three calculated quantities: the fuzzy performance index, the modified partition entropy and the separation distance (Mahmoodi, 2016). Figure 6 and 7 show the geologically logged rock types with the measured parameters and clustering results for FNX 1182 and FNX 1168 respectively. Both drillholes have numerous heterogeneous zones with high confusion indices. The corresponding samples collected from these heterogeneous areas will be discussed to show that changes in physical properties are reflective of the geology.

Drillhole FNX 1168 frequently has areas of missing core, therefore, samples prior to 851.2 m will not be discussed with the exception of metabasalt schist (the location is marked with label A to the left of the geologic log). The most homogenous zones are within the olivine diabase around 858.3 m (label B) and a narrow zone at 919.7m, with a low confusion index of 0.06. Quartz diorite is consistently well classified into cluster 4, with the exception of 2 local heterogeneities at 880.02 m, where the confusion is high (0.92) and the sample has been classified into cluster 2 due to a higher count in K and small increase in eU and eTh (label C). Also at 899.6 m, there is an increase in magnetic susceptibility and density, with a decrease in all gamma counts, particularly the K counts (label D), resulting in a high confusion index (0.81).

Near the end of the hole, the metagabbro and metasediment show several small fluctuations in confusion index due to frequent changes in physical parameters, with metagabbro poorly classified into cluster 3 (label E) and metasediment classified into cluster 2 (label F). Going downhole approaching the metagabbro-metasediment contact, all gamma counts increase, while the density and magnetic susceptibility decrease, classifying the sample into cluster 4 (label G) which transitions below into cluster 2 when the hole is in the metasedimentary rocks.

In FNX 1182, the confusion index is generally high caused by the relatively high heterogeneity within the rock units. Quartz diorite has a low confusion index when it is classified into cluster 2 at 820.4 m, 870.6 m, 894.9 m (label H), and 927.8 m, where total gamma counts increase from 1800-1900, up to 2100-2500. However, the quartz diorite is also classified into cluster 4 and in some cases into cluster 3, generally where the confusion index is high (0.85). For example, around 1052.2 m, there are increases in density and slight decreases in gamma readings (label I). The quartz diorite-metabasalt contact (label J) and the quartz diorite unit (label K) are highly confused when there are increases in the conductivity, magnetic susceptibility and density.

In addition, at the end of the hole (label L), the pyroxenite, metagabbro and metabasalt show similar physical properties. Metagabbro at the top of the hole (label M) increases in K and eU, and is classified into cluster 2, where metagabbro at the bottom of the hole has lower K readings and is well classified as cluster 3 (figure 8).

The poor classification results in this hole are interpreted to be due to erratic behavior in the three gamma-ray readings resulting in high confusion indices. The density and magnetic susceptibility seems to distinguish the quartz diorite and the inclusion quartz diorite from each other as the inclusion quartz diorite has narrower properties than quartz diorite (figure 5).

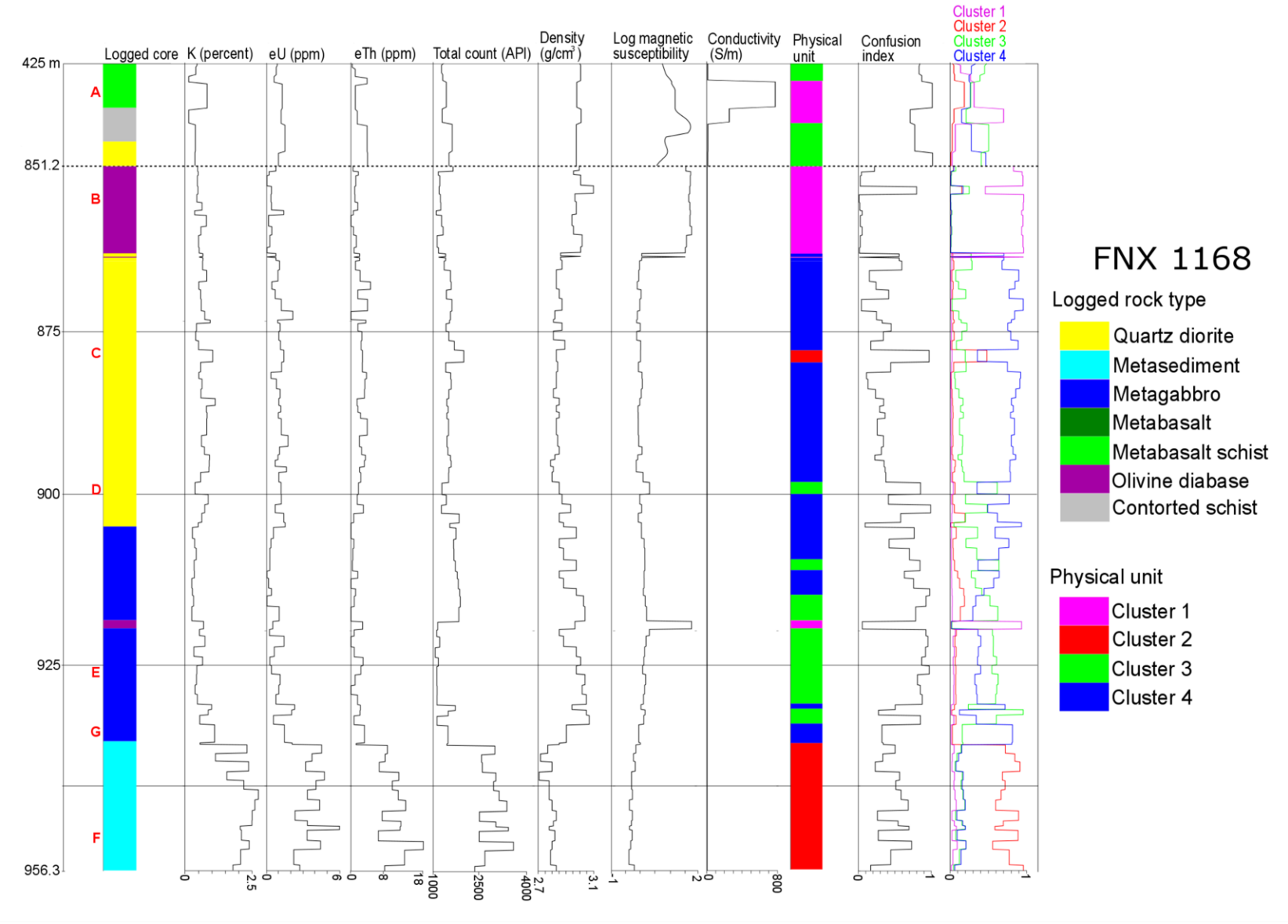

Figure 6: Results of clustering FNX 1168 with logged rock type, K (percent), eU, eTh (ppm), total count, density, magnetic susceptibility, conductivity and clustering results: physical units, confusion index and membership for clusters.

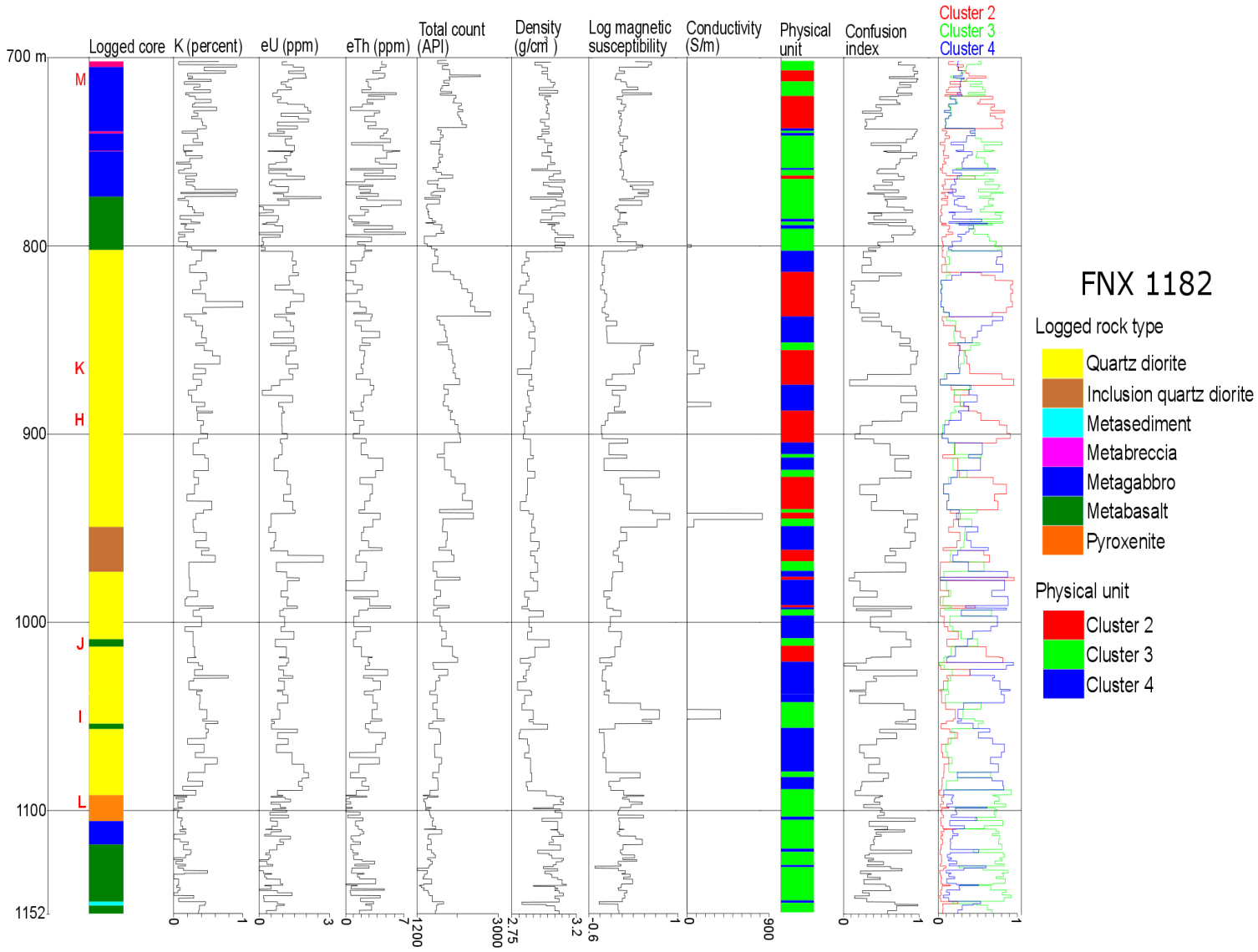

Figure 7: Results of clustering FNX 1182 with logged rock type, K (percent), eU, eTh (ppm), total count, density, magnetic susceptibility, conductivity and clustering results: physical units, confusion index and membership for clusters.

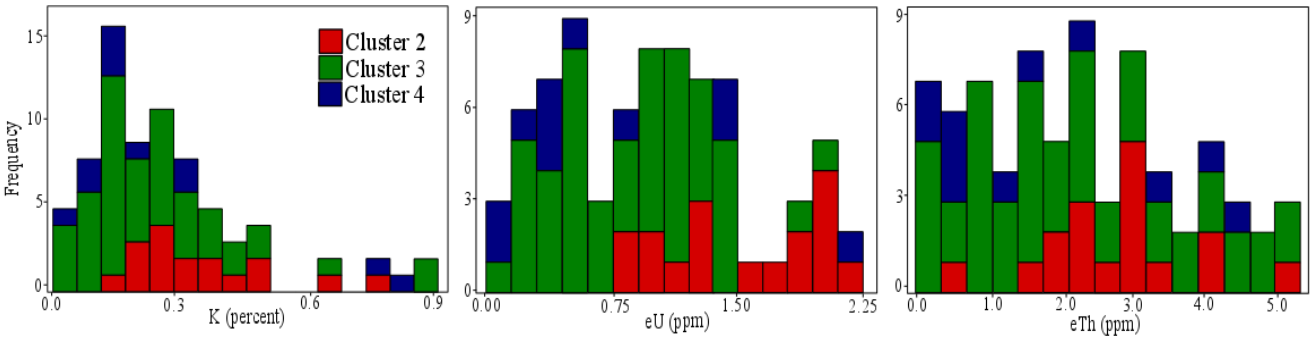

Figure 8: Histograms of metagabbro samples for K (%), eU and eTh (ppm).

4.4 Mineralogy

Olivine diabase is black, medium-grained with a consistent mineral assemblage of plagioclase, pyroxene, olivine, magnetite and ±biotite. There is no visible alteration and the unit has 2 m wide chilled margins at the beginning and end of the unit. Contacts are irregular and sharp. No sulphide or economic mineralisation is evident in the olivine diabase.

Metasediment is a light gray, fine-grained, with muscovite, plagioclase, quartz, amphibole, ±biotite, opaques with locally visible zircon grains under the microscope. Samples lack bedding features and have coarse crystals of amphibole in samples found in FNX 1168. No sulphide or economic mineralisation is found.

Metagabbro, metabasalt and pyroxenite are light to dark gray with amphibole, plagioclase, quartz, opaques, epidote/zoisite ±biotite, and ±calcite. Pyroxenite has coarse grains of amphiboles, about 0.1-0.5 mm in diameter. Pyroxenite gradually transitions to the metagabbro in FNX 1182, as the crystals of amphibole decrease and become less prevalent. Metabasalt is fine-grained and amygdaloidal with gradual contacts with the metagabbro. In FNX 1168, no pyroxenite was found, but metabasalt in FNX 1168 is similar to that in FNX 1182, with the

exception of the top of the hole where there is highly sheared and mineralised metabasalt schist. All three units have weak-pervasive chlorite, epidote and carbonate alteration, with some areas of possible biotite alteration concentrated within the metagabbro. Samples of metagabbro and metabasalt with pervasive chlorite alteration have a distinct green-tint in hand sample. Chalcopyrite, pyrite, pyrrhotite mineralisation ranges locally between 0-10% in the metagabbro and metabasalt, however, it is mostly barren. The pyroxenite unit shows no sulphide or economic mineralisation, with the exception of some pyrrhotite mineralisation at the gradual contacts between the metagabbro and metabasalt units.

Quartz diorite is light gray, medium grained with plagioclase, quartz, biotite, amphibole, ±zoisite/epidote, ±opaques, and ±calcite, where the opaques consist of pyrrhotite, chalcopyrite and pyrite. These opaques are more abundant in the quartz diorite than any other rock type, ranging from 0-50%. Moderate to pervasive alteration occurs as carbonate, epidote and chlorite. In FNX 1182, there are sporadic areas with metabasalt inclusions.

The inclusion quartz diorite in FNX 1182 appears similar to the quartz diorite unit, but has more abundant (~15-20%) mafic inclusions; however, the transition between quartz diorite is gradual with the highest concentration of mafic inclusions between 949.5-973.3 m in FNX 1182. Figure 9 outlines the three clusters that quartz diorite is classified into, where the differences between the three physical units are best seen in the magnetic susceptibility (clusters 2 and 4 have lower values), density (cluster 3 has higher values) and eU (cluster 3 has lower values and cluster 2 higher values) with less discernable differences in K and eTh.

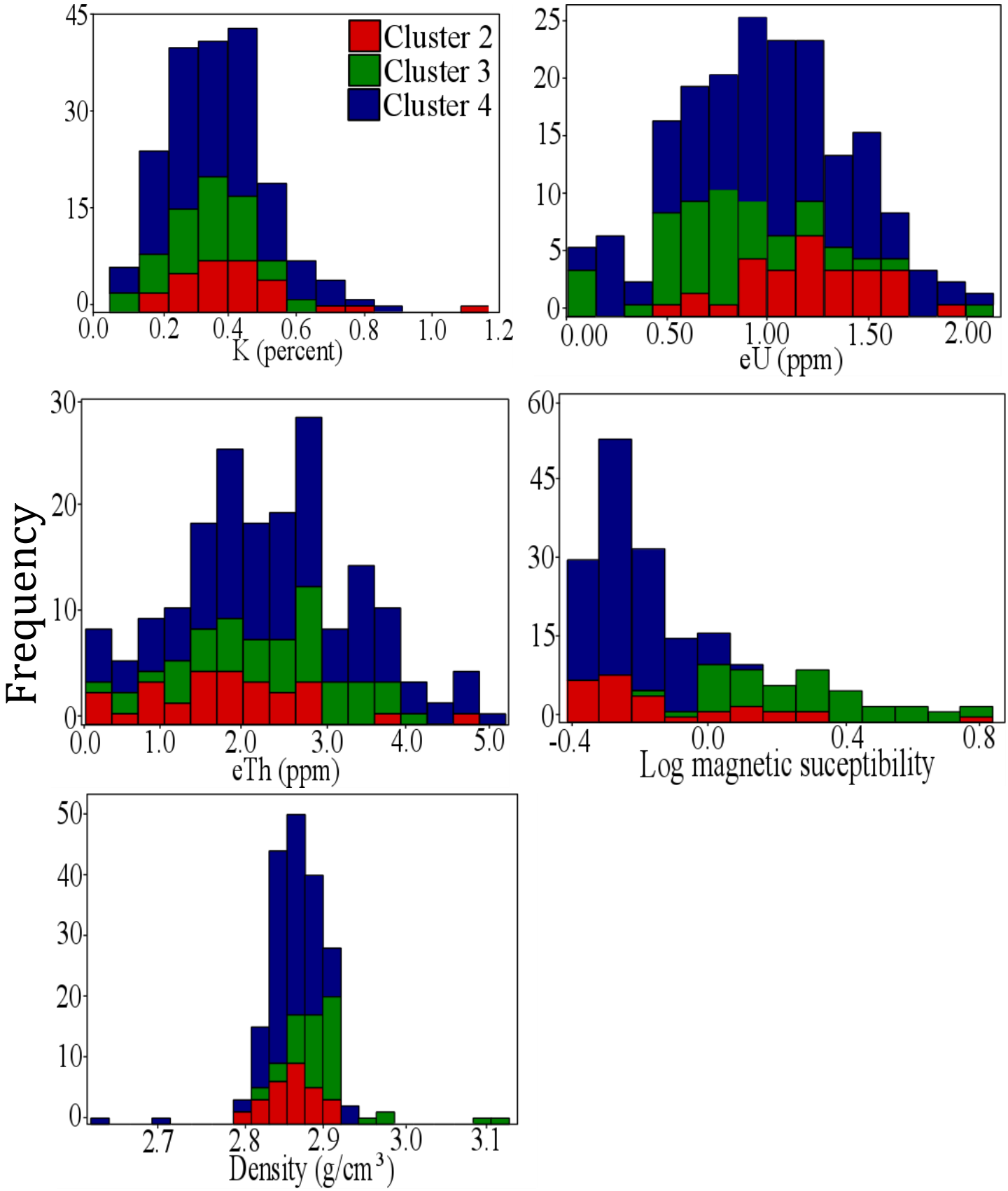

Figure 9: Histograms of quartz diorite and inclusion quartz diorite for K (%), eU (ppm), eTh (ppm), density (g/cm^3) and the log of magnetic susceptibility

FNX 1168	**Amp**	**Bt**	**Chl**	**Epi/Zoi**	**Carb**	***Opaques**	**Plag/Qtz**	****Visible Zir**	**Musc**
MTBS (426.2 m)	20	15	10	12	0	18	25	0	0
QD (819.5 m)	0	10	23	20	0	15	30	trace	2
MTGB (929.7 m)	25	10	15	10	trace	10	30	0	0
MTGB (935.8 m)	18	20	15	13	0	5	30	0	0
MTSD (952.8 m)	0	0	15	0	0	12	25	3	45
FNX 1182	**Amp**	**Bt**	**Chl**	**Epi/Zoi**	**Carb**	***Opaques**	**Plag/Qtz**	****Visible Zir**	**Musc**
MTGB (746.4m)	35	45	trace	0	trace	7	13	0	0
MTGB (753.4m)	30	23	7	5	5	10	20	0	0
MTGB (759.7m)	0	0	35	15	17	8	25	0	0
MTBS (771.5m)	30	35	15	5	trace	trace	15	trace	0
MTBS (789.2m)	33	5	15	10	2	5	30	trace	0
MTBS (793.8m)	40	14	20	0	0	trace	25	1	0
QD (862.4m)	20	25	10	5	trace	10	30	trace	0
QD (894.9m)	20	25	10	7	0	7	30	1	0
IQD (961.6m)	15	25	15	5	0	10	30	trace	0
QD (983.1m)	20	23	15	10	0	7	25	trace	0
QD (1052.2m)	40	20	10	trace	0	5	25	trace	0
QD (1061.4m)	20	25	8	5	0	10	30	2	0
PYRT (1092.8m)	45	2	0	10	1	10	30	3	0
PYRT (1095.3m)	40	trace	10	8	7	10	25	0	0
MTGB (1112.2m)	60	trace	7	5	10	3	15	trace	0
MTGB (1115.1m)	60	2	7	3	3	5	20	trace	0
MTBS (1118m)	60	trace	0	10	0	10	20	1	0
MTBS (1142.3m)	60	trace	7	trace	0	8	25	trace	0

Table 6: Mineral percentage for different samples; * pyrrhotite, chalcopyrite, pyrite, magnetite and pentlandite; **equal to or greater than 0.02 mm

5 Discussion

5.1 Physical units and rock units

Cluster 1 are primarily olivine diabase, which are highly magnetic and dense samples with low gamma readings. They are composed of Fe-Mg rich minerals, resulting in a high density and magnetic susceptibility. Their distinct characteristics allow the olivine diabase to be well classified into cluster 1, which is comparable to the cluster identified by Mahmoodi (2016) as the HighMag cluster.

Metasedimentary samples are primarily classified into cluster 2, characterized as high total gamma count, low density and low magnetic susceptibility, poor in ferromagnesium minerals and rich in felsic minerals with K, Ca and Si. High gamma is common in sedimentary rocks containing zircon, which carry incompatible large-ion lithophile3 elements like U and Th (Shives, 2015).

Metagabbro, metabasalt and pyroxenite are most frequently classified into cluster 3, where gamma readings are low, while the density and magnetic susceptibility is high, but lower than cluster 1. Low gamma readings are consistent with the composition of these samples due to a greater portion of mafic minerals.

Quartz diorite is primarily classified in cluster 4, where density, magnetic susceptibility and gamma readings are moderate. Physical property changes in the quartz diorite tend to be variable as a consequence of the presence or lack of sulphide minerals and the fact that the quartz diorite is an intrusive body within the basaltic country rock, incorporating mafic xenolith inclusions, which change the physical properties, primarily magnetic susceptibility and density; however, there simply is not enough inclusion quartz diorite samples to define another cluster. Inclusion

quartz diorite has a matrix similar to quartz diorite but has mafic inclusions of what appears to be xenoliths of metabasalt, causing the confusion index to be persistently high (0.61-0.95).

5.2 Correlation of heterogeneities and geology

From Table 5, every rock unit, with the exception of olivine diabase, belongs to more than one cluster and thus shows heterogeneities in physical properties, which can be a representation of changes in their mineral assemblage. Observations drawn from the core from the Victoria property suggest that rock units acquire characteristics of other rocks that create confusion in the algorithm.

5.2.1 Mineralisation

Quartz diorite shows the most variability in cluster classification, primarily as a consequence of chalcopyrite, pyrrhotite, and pyrite mineralisation (figure 10), which creates a high confusion index in cluster 3. Highly mineralised samples are denser, have an increase in magnetic susceptibility (pyrrhotite) and can even have enough continuity in the chalcopyrite and or pyrrhotite to produce an elevated conductivity reading, causing the algorithm to confuse it with something more physically similar to a rock like metagabbro. Similarly, the metabasalt has areas of abundant pyrite mineralisation, where the metabasalt schist is poorly classified in cluster 1 (figure 11).

A high confusion index might indicate transition zones where there is a boundary between 2 different clusters because boundaries between units are not always sharp but can be gradual (Mahmoodi and Smith, 2015). Not only is a transition between quartz diorite and metabasalt in FNX 1182 at 1010.5 m indicated by a high confusion caused by inclusions of metabasalt in the quartz diorite as you approach the gradual contact, but gradual changes in mineralisation have

created zones of high confusion within the quartz diorite units (899.6 m) and the contorted metabasalt schist (426.2 m).

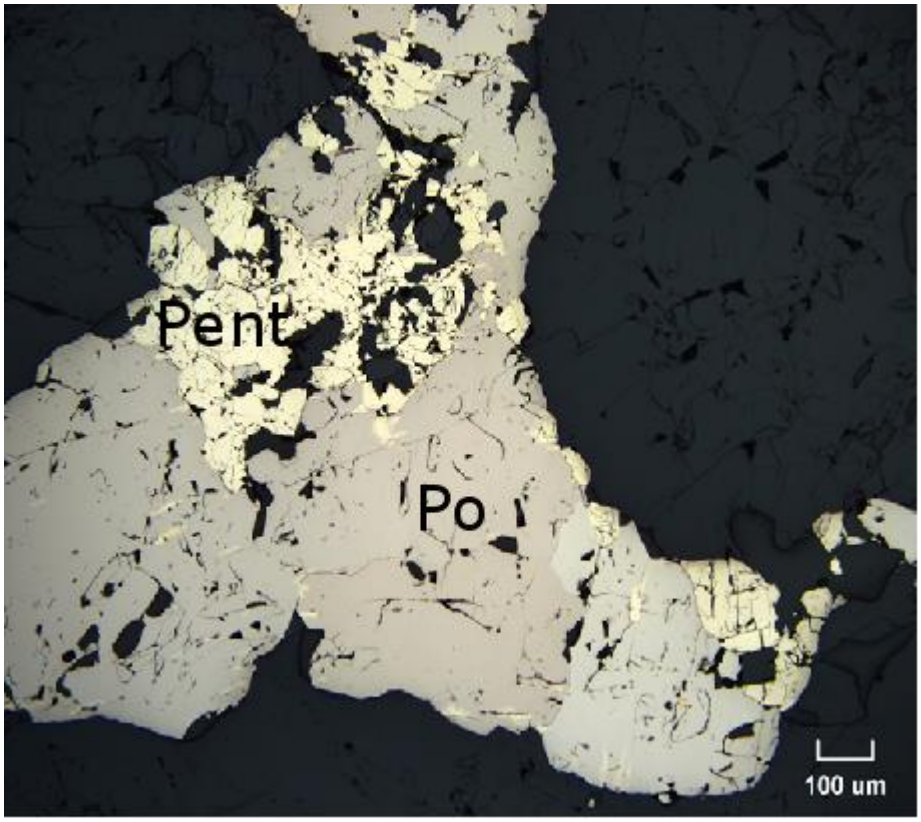

Figure 10: Photomicrograph of mineralised (Pent and Po) quartz diorite from FNX 1168.

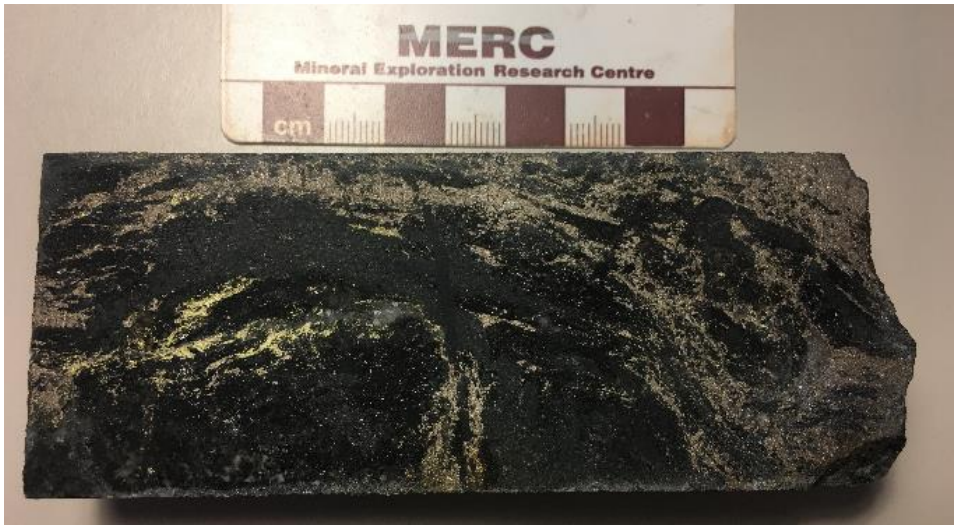

Figure 11: Photo of contorted metabasalt schist from FNX 1168

When the cluster classification of a unit changes as a consequence of changes in the extent of mineralisation, the confusion index increases because there is a decrease and/or increase in two or more membership values. These highly confused mineralised zones are categorised into narrow zones with an anomalous cluster classification, as physical property variations occur in a narrow zone.

The conductivity shows some distinct highs, which could be manually classified into a “high conductivity” cluster rather than be paired with certain rock types.

5.2.2 Variation of rock-forming minerals

Variability in the proportions of the more common rock-forming minerals (silicates) within identical rock units can cause small fluctuations in the confusion and even change physical properties enough for them to be confidently classified into different clusters. Metagabbro and quartz diorite (normally in clusters 3 and 4) have this property, where they both have occurrences found within cluster 2. Figure 12 shows two petrographic photos under plane polarised light of the metagabbro at 746.4 m in FNX 1182 (figure 12A) at 1108.1 m (figure 12B). There are two distinct groups of metagabbro that can be documented in the physical measurements and core samples: biotite-rich metagabbro in cluster 2 (figure 12A) and biotite barren metagabbro from cluster 3. This increase in biotite causes the increase in K signature, increasing the gamma reading whereas the trace biotite metagabbro has lower K readings. However, this increase in biotite content does not always increase the confusion index, for example the confusion index stays low (0.3-0.4) when classified into cluster 2. This is an effect of many physical properties being affected by an increase in K content: density decreases and total count increases. These property changes shift the sample from cluster 3 to cluster 2, explaining the low confusion index.

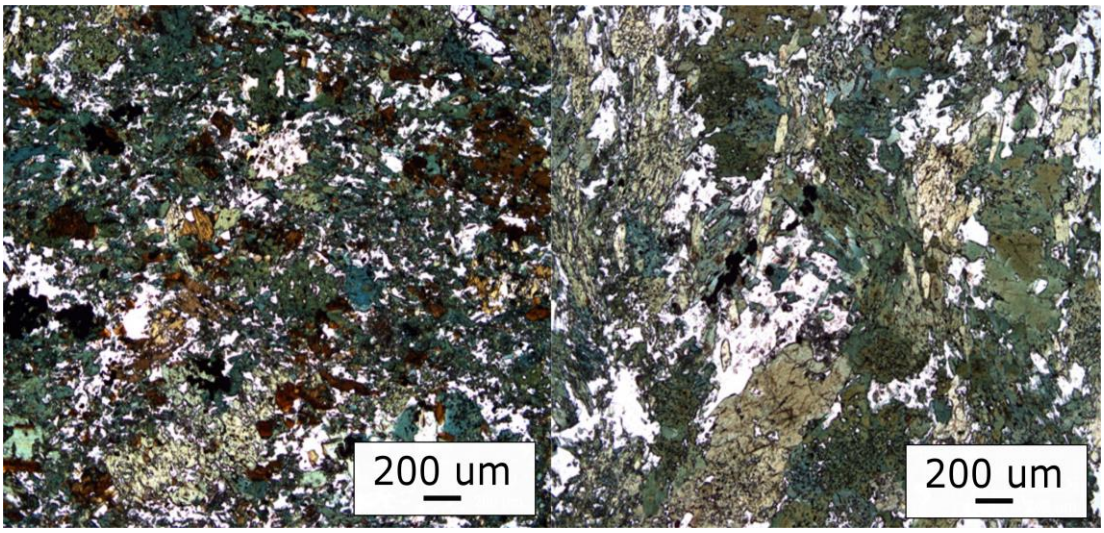

Figure 12: Photomicrographs images from FNX 1182: (A) Biotite-rich metagabbro at 746.4 m (K = 0.42%), C.I. = 0.36; (B) Biotite barren metagabbro at 1108.1 m (K = 0.10%), C.I. = 0.34.

All three mafic units (metagabbro, metabasalt and pyroxenite) commonly have accessory phases like zircon and apatite that can increase the eU and eTh assays. Increases in eU and eTh in these units caused by zircon content are large enough to change the total gamma count and cause overlap with a unit demonstrating higher total gamma count than a mafic unit (metasedimentary rock, quartz diorite), resulting in a high confusion index.

For quartz diorite, mafic inclusions (figure 13) increase the density and magnetic susceptibility and decrease the total gamma count slightly, causing it to be classified into cluster 3 when mafic inclusion abundance increases. The quartz diorite that is classified into cluster 2 shows only subtle mineralogical changes.

Figure 14 shows cross-plots of the metasedimentary rocks (circles) and quartz diorite (triangles) classified into cluster 2 (red) and cluster 4 (green). The metasedimentary rocks only occur in cluster 2 (red circles) but quartz diorite has been classified as cluster 2 and 4. The segregation between 2 and 4 is sharp and occurs because cluster 2 samples have a total count higher than

2000, whereas cluster 4 samples do not. The quartz diorite is an intrusive that cuts into Paleoproterozoic Huronian metavolcanics and metaseidmentary rocks (Lightfoot and Farrow, 2002). Mafic inclusions are easily seen in the core; however, inclusions of metasedimentary rocks are likely in the quartz diorite, they are just very difficult to see as they are mineralogically similar to quartz diorite. As a result, increasing the concentration of metasedimentary inclusions in the quartz diorite causes the quartz diorite to have a signature similar to metasedimentary rock (cluster 2).

In this case it seems that the fuzzy k-means classification is relying on total count to separate classes, perhaps because the number of samples is dominated by quartz diorite and metasedimentary rocks are not statistically significant. Looking at the cross plots in figure 14, the metasedimentary rocks do appear to have a distinctly different character from the quartz diorite. The metasedimentary rocks have consistently higher K, eU and eTh and a slightly lower magnetic susceptibility. Even the density is lower in the metasedimentary samples. It is not clear why the fuzzy k-means algorithm did not classify these red circles as a separate cluster, but it is likely because there are a small number of metasedimentary rock samples. Although metasedimentary rocks have high assay gamma readings, abnormally large readings of eTh (eTh >12 ppm), causes a high confusion index.

Although logged as two different units, quartz diorite and inclusion quartz diorite appear in this study to be quite similar except where the appearance of inclusions within the quartz diorite is concentrated, for example between 949.5-973.3 m. Inclusion quartz diorite consistently has a high confusion index because the matrix contains mafic inclusions, much different from quartz diorite.

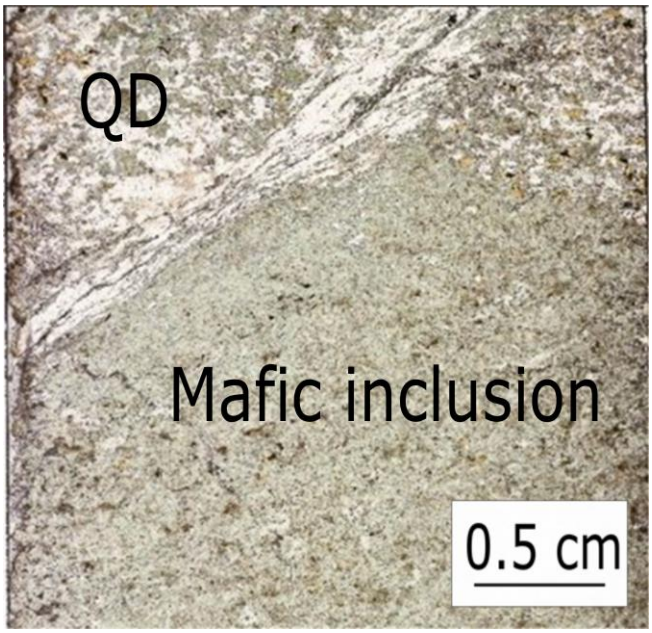

Figure 13: Photomicrograph in plane polarised light of inclusion quartz diorite with a mafic inclusion in a quartz diorite matrix.

5.2.3. Effect of zircon

Gamma signature is variable in all rock types. Quartz diorite and metasedimentary rocks are felsic rocks have a higher gamma signature than mafic rocks, metabasalt, metagabbro and pyroxenite. Proportions of zircon did vary in all these rocks types. Zircon can contain elements Th and U, which can be measured. Anomalously high gamma signatures were primarily evident in the mafic rocks and corresponded to zircon proportions.

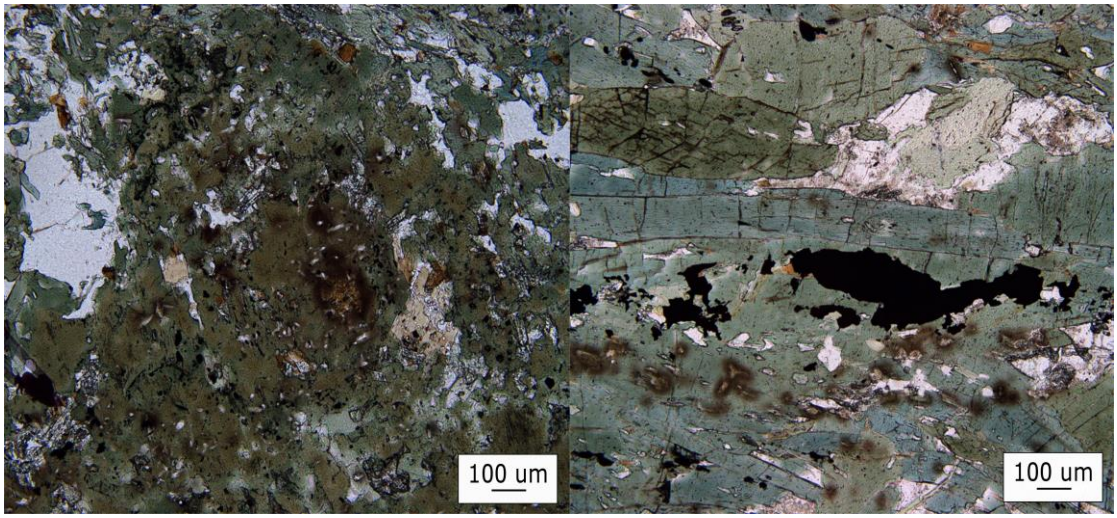

Figure 14: Photomicrographs of: (A) metabasalt with a eTh value of 6.23 ppm and C.I. = 0.92 (B) pyroxenite with an eTh value of 2.2 ppm (C.I.=0.48)

However, these mafic rocks typically have low gamma assays, therefore increasing the gamma increases the confusion index. Figure 14 shows zircons in metabasalt and pyroxenite, with eTh values elevated from the average value. Increases in zircon proportions and grain size caused rocks like metabasalt and pyroxenite to have higher than usual gamma values and increased their confusion index, due to overlapping in clusters 3 and 4.

5.3 Correlation of homogeneity and geology

Textural changes result in a corresponding change in rock names, for example the grain size being used to distinguish between coarse-grained gabbro and fine-grained basalt; however, this should not change the physical signature of the rocks since they are mineralogically similar, except for their grain size. As seen above with homogeneities, variations in mineral proportions and sulphide minerals can alter parameters like density and magnetic susceptibility. This is seen

a few times in metagabbro, metabasalt and pyroxenite, but at the base of drillhole FNX 1182, all three rock types are well classified into cluster 3. In hand sample (figure 15), these three rocks look very similar, with the exception of porphyroblasts of amphibole in the pyroxenite. In their corresponding photomicrographs, all three units have amphiboles instead of pyroxenes with varying grain size.

The rock unit logged as “pyroxenite” contains porphyroblasts of amphiboles, with the grain size of the porphyroblasts decreasing as you approach the metagabbro and metabasalt with transitional contacts. Mahmoodi and Smith, 2015 speculated that the pyroxenite is primarily made of mafic mineral pyroxene, causing it to easily be misclassified as a metagabbro or a basalt. Furthermore, these three units likely started as a basalt protolith (which can have pyroxene), but contact metamorphism from the quartz diorite intrusion resulted in the rock being recrystallized and forming amphibole porphyroblasts. More suitable names for these units would be amphibole granofels (for the rock type logged as pyroxenite) and amphibole hornfels (for the rock types logged as metagabbro and metabasalt).

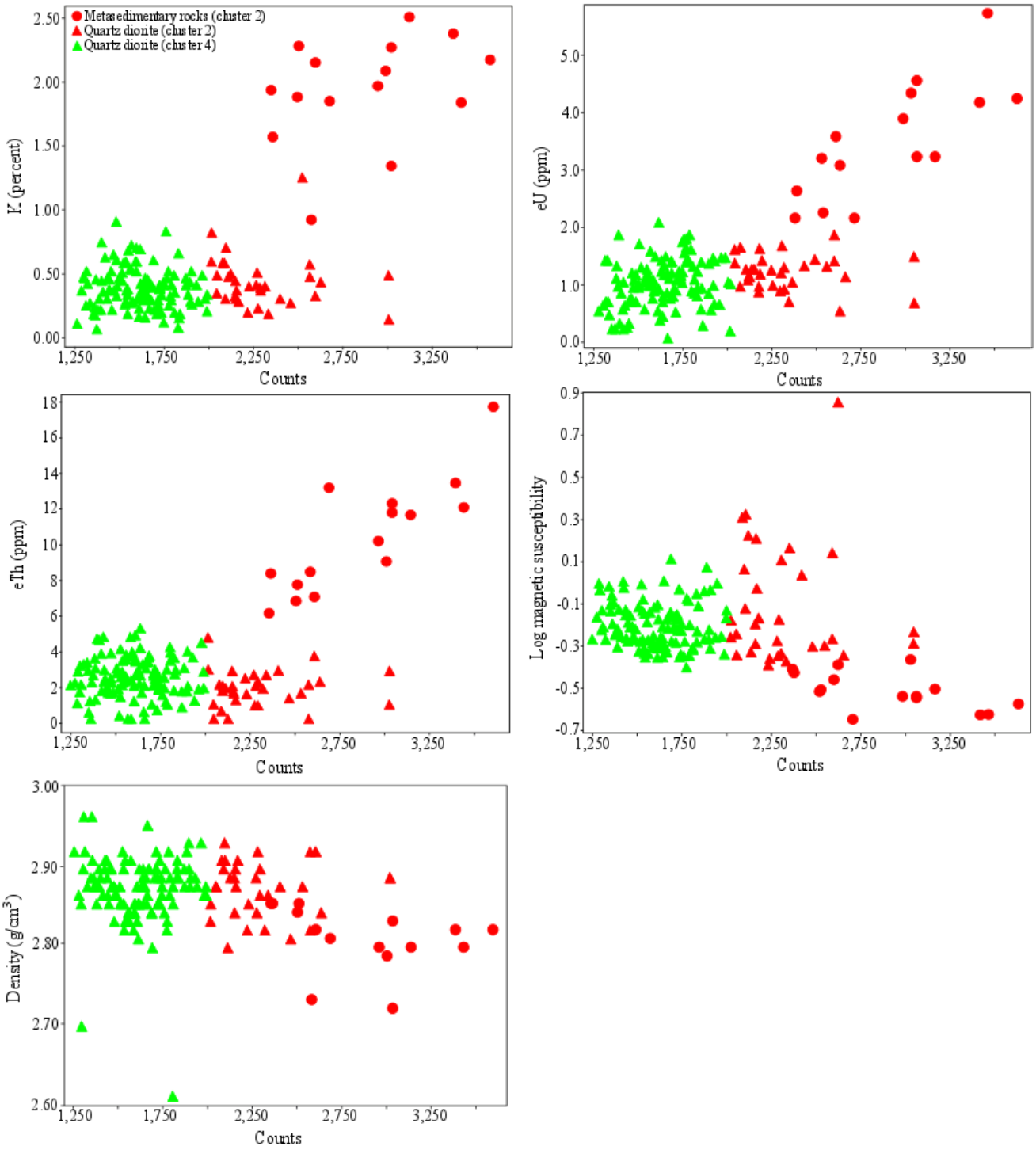
Metasedimentary rocks (cluster 2)
Quartz dionite (cluster 2)
Quartz dionite (cluster 4)
K (percent)
eU (ppm)
eTh (ppm)
Log magnetic susceptibility
Density (g/cm3)
Counts
1,250
1,750
2,250
2,750
3,250

Figure 15: Samples of quartz diorite (triangles) and metasediment (circles). In all cases the horizontal axis is total count, with 2000 counts forming the distinction between cluster 2 and 4. Samples classified into cluster 2 are red and cluster 4 is green.

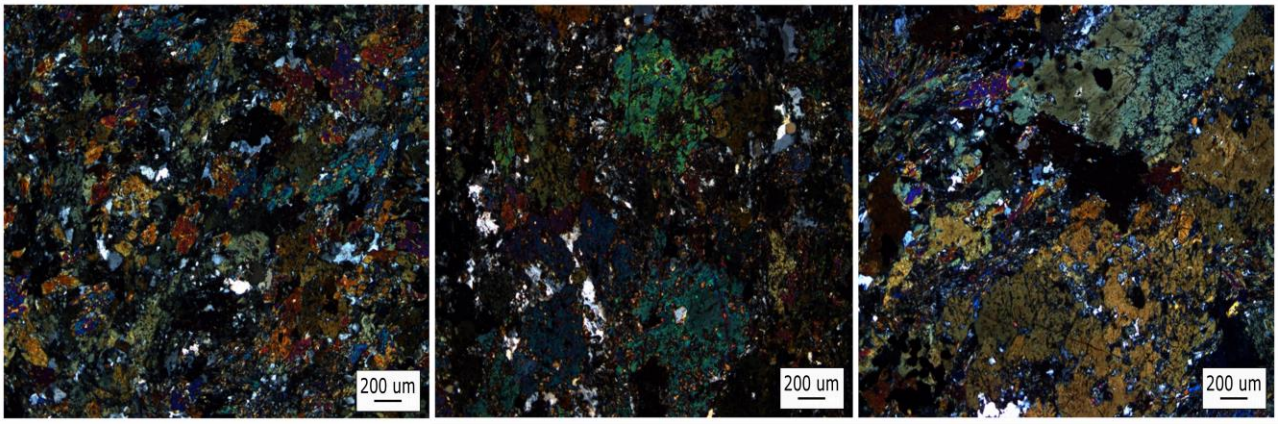

Figure 16: Photomicrographs of metabasalt, metagabbro and pyroxenite (left to right) from FNX 1182.

5.4 Total count vs. K, eU and eTh readings

In the study done by Mahmoodi and Smith (2015), the information available was the downhole total gamma count. In this study, the K, eU and eTh GRS assays were estimated from the additional windows in the RS-330 gamma ray-spectrometer. In cases where there are total count changes, the individual element gamma counts were helpful in accounting for the change in total count. For example, the biotite-rich metagabbro showed an enhanced total count, which can be attributed to the increase of K in biotite.

In other cases, there were not clear and coherent changes in the individual elements that seemed to have geological significance. In very general terms, an increase in one GRS measure correlates with all other GRS measures increasing, so perhaps the fuzzy k-means lumped the GRS measures all together in a statistical sense. However, in detail there are many cases evident on figures 5 and 6, where one GRS measure decreases and one or more other increases.

Hence there is geological information available, but the fuzzy k-means does not seem able to extract it. Other examples of information being in the GRS assays are seen on Figure 8 and 9, where individual radioelements seemed to have individual behavior distinct from other radioelements, implying there is geological information in the radioelement variation.

Separate elements were able to distinguish between quartz diorite and metasediments, but it seems the statistics were inadequate in distinguishing a clear change for the total counts, as seen in the quartz diorite in cluster 2 versus quartz diorite in cluster 4 (figure 14). Figure 16 shows that denser, mafic units have a lower total count, while felsic, less dense units have higher total counts; however, the statistical sample of felsic units is once again small. In order to see a clear change in one or more of the estimated K, eU and eTh, there must be a distinct change in mineral assemblage, unfortunately quartz diorite and metasediment are mineralogically similar, thus no differences are observed.

Mahmoodi (2016) found weaknesses in the fuzzy k-means classification in identifying statistically small clusters such as those with high magnetic susceptibility. This weakness was overcome by manually assigning these to a manually added cluster called “himag”. It seems with the GRS data, there could be similar issues, highlighting a need to generate separate manual classes with high or low values of GRS assays.

Further work could be to try the clustering on a larger data set that has more statistical samples. Other avenues for research are to look at radioelement ratios rather than the assays to see if there is geological information that can be extracted from the ratios. A different approach could be to investigate other machine learning methods that might be able to identify clusters with a smaller number of samples.

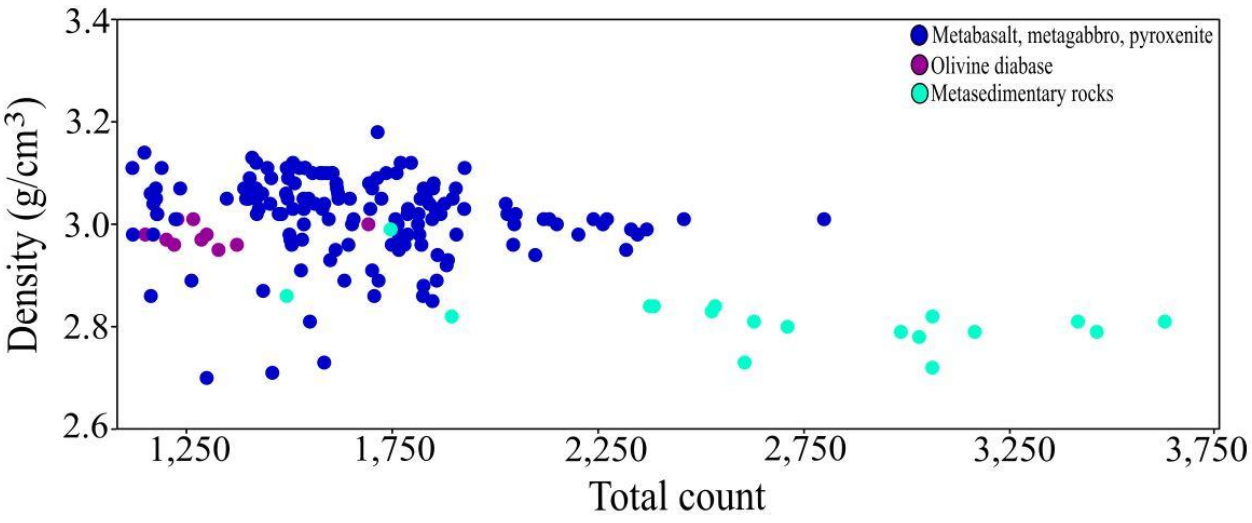

Figure 17: Cross plot of density against total count for most mafic samples measured (olivine diabase, metagabbro, metabasalt and pyroxenite) with most felsic samples measured (metasedimentary rocks).

5.5 Comparision of downhole logs and surface logs

The difference between downhole logs and surface logs were not too different. Since downhole logs are continuous, there is more consistent and accurate data than surface logs taken every 0.5-1 m apart. The surface logs provided more information with the gamma ray assays, allowing changes in separate assays of K, eU, and eTh, for examples specific spikes in K corresponded to the biotite alteration in metagabbro. In addition, going downhole, restricts the size of your instrument. For example, a small crystal would be needed for a drillhole, however, on surface, crystal size is not restricted and can thus provide better gamma ray assays

6 Conclusion

The fuzzy-k means algorithm is successful in classifying zones of heterogeneities and homogeneity using physical property measurements obtained on core samples from the Victoria property. The algorithm found 4 physically different clusters to categorise the 6 different rock types measured. The more homogenous units have consistent mineral assemblages, like the olivine diabase and metasediment. Both of these units show only small changes in density, magnetic susceptibility and gamma signature because of their relatively minor changes in mineral proportions. As a consequence, their classification is straightforward and they have low confusion indices.

The other rock units have variable proportions of minerals in different zones and are thus heterogeneous, causing their physical properties to vary enough that they were classed into different clusters. The mineralised, dense samples of quartz diorite classify as cluster 3, where less dense and unmineralised quartz diorite is classified as cluster 4, or as cluster 2 when total gamma counts increased. It is difficult to determine whether these changes in cluster are caused by changes in the K, eU and eTh, as the change is subtle. The pyroxenite, metagabbro and metabasalt units were generally all categorised into the same cluster. This is consistent with the thin section study, which showed all three units to be identical in mineral assemblage, with only the grain size showing a decrease as you approach the end of the hole. Petrology suggested that the samples logged as pyroxenite, metagabbro are actually amphibole granofels into amphibole hornfels. These are likely derived from a basaltic protolith, which underwent contact metamorphism from the quartz diorite intrusion. This is consistent with the metabasalt inclusions evident in intervals within the quartz diorite.

The workflow from Mahmoodi and Smith, 2015 was helpful in categorising the heterogeneous units. To organize the representative samples discussed above, the samples with high confusion were put into each of the following categories:

1) Local heterogeneities where mineral assemblages changed subtly with slight changes in the gamma, density or magnetic signature. Frequently seen with quartz diorite where variable ore mineralisation creates local changes within the units.
2) New class zones due to significant changes in a physical property, but the number of samples is too small to create a distinct statistically identifiable class. For example, the highly magnetic samples that are evident in the metabasalt schist, contorted schist, and highly mineralised quartz diorite that have high conductivity readings. Other narrow zones of high confusion were numerous, particularly at the top and bottom of hole FNX 1182, but it was not clear which physical property variations these were associated with.
3) Transition zones with gradational changes from one zone to another. For example from unmineralised zones to mineralised zones within quartz diorite, metagabbro and metabasalt, quartz diorite to metabasalt contacts, quartz diorite to pyroxenite contact, and the metagabbro to metasediment contact.
4) Intermediate zones where mineral proportions caused an increase or decrease in physical properties like eTh and eU. For example, increased zircon content seen within metagabbro, metabasalt, pyroxenite, metasediment and quartz diorite.

The areas of high confusion were a great way to select core for further geological investigation in order to understand the relationship between rock classification and physical properties.

References

Benaouda, D., Wadge, G., Whitmarsh, R., Rothwell, R. G., & MacLeod, C. (1999). Inferring the lithology of borehole rocks by applying neural network classifers to downhole logs: an example from the Ocean Drilling Program. *Geophysics Journal International, 136 (2),* 477-491.

Lightfoot, P. C., & Farrow, C. E. (2002). Geology, geochemistry, and mineralogy of the Worthington offset dike: A genetic model for offset dike mineralization in the Sudbury Igneous Complex. *Economic Geology, 97*(7), 1419-1446.

Erdi-Krausz, G., Matolin, M., Minty, B., Nicolet, J. P., Reford, W. S., & Schetselaar, E. M. (2003). *Guidelines for radioelement mapping using gamma ray spectrometry data*. International Atomic Energy Agency (IAEA).

Mahoomdi, O. (2016). *Application of Physical Properties Measurements to Lithological Prediction and Constrained Inversion of potential field data, Victoria Property, Sudbury, Canada.* PhD Thesis. Laurentian University

Mahoomdi, O., & Smith, R. (2015). Clustering of downhole physical property measurements at the Victoria property, Sudbury for the purpose of extracting lithological information. *Journal of Applied Geophysics*, 145-154.

Mahoomdi, O., Smith, R., & Tinkham, D. (2015). Supervised classification of down-hole physical properties measurements using neural network to predict lithology. *Journal of Applied Geophysics, 118,* 17-26.

Rousell, D. H., & Card, K. D. (2009). Sudbury area geology and mineral deposits. *A Field Guide to the Geology of Sudbury, Ontario, 6243*, 1-6.

Shives, R.B.K., 2015. Using gamma ray spectrometry to find rare metals. In: Simandl, G.J. and Neetz, M., (Eds.), Symposium on Strategic and Critical Materials Proceedings, November 13-14, 2015, Victoria, British Columbia. British Columbia Ministry of Energy and Mines, British Columbia Geological Survey Paper 2015-3, pp. 199-209.

Spicer, B. (2016). Geophysical signature of the Victoria property, vectoring toward deep mineralization in the Sudbury Basin. *Interpretation*, 281-290.

Žalik, K. R. (2008). An efficient k'-means clustering algorithm. *Pattern Recognition Letters, 29 (9)*, 1385-1391.